Batch adsorption of fluoride ions onto microwave assisted activated carbon derived from Acacia Auriculiformis scrap wood

Monal Dutta, Tanumoy Ray, Jayanta Kumar Basu*

Department of Chemical Engineering, Indian Institute of Technology, Kharagpur, India

_____

ABSTRACT

Adsorption of fluoride was done from its aqueous solution by using microwave assisted activated carbon. The activated carbon was prepared by carbonization of Acacia Auriculiformis scrap wood char followed by microwave heating. A batch study on fluoride sorption was carried out at various experimental conditions, including different pH, initial fluoride concentrations, adsorbent concentrations, competitive anion chloride and different temperatures. Fluoride adsorption was found to be pH dependent and the maximum removal of fluoride was obtained at pH of 4.4. On the other hand, the fluoride adsorption was reduced in the presence of chloride ions. The percentage removal of fluoride was found to be increased with increase in temperature and adsorbent dose and a maximum removal of 97.2% was obtained with an adsorbent dose of 2 g/l. On the other hand, the adsorption of fluoride was also increased with decrease in particle size and the maximum removal occurred at a particle size of 58 μm. In order to investigate the mechanism of fluoride removal, various adsorption isotherms such as Langmuir, Freundlich, Tempkin and Herkin-Jura were fitted at 293, 303, and 323 K . The experimental data revealed that the Langmuir isotherm gave more satisfactory fit for fluoride removal. The monolayer adsorption capacity according to Langmuir isotherm was found to be 19.92 mg/g. The adsorption process was observed to follow a pseudo-second-order kinetic model. Thermodynamic parameters were also determined and change in enthalpy and entropy were found to be 6.094 kJ/mol and 19.022 J/mol-K respectively.

Keywords: Adsorption; Mean square error; Sum of square error; Chi-square, Regression coefficient.

_____

INTRODUCTION

Adsorption of hazardous ions such as fluoride has become major concern for public health in the present decade. Unfortunately, the fluoride contamination of ground water has been identified in many places around the world [1]. The natural presence of fluoride generally occurs through soil and rock formation in the form of fluorapatite, fluorspar and amphiboles, geochemical deposits, natural water systems and earth crust [2, 3]. In addition to this fluoride can also be found in

536

various industrial activities, specially semiconductor, electroplating, glass, steel, ceramic and fertilizers industries [4]. According to the World Health Organization (WHO) the maximum permissible limit of fluoride is 1.5 mg/l in case of drinking water whereas the acceptable fluoride concentration lies in the range of 0.5 - 1.5 mg/l as per the APHA standards. Therefore higher fluoride concentration cause severe harmful effects in aquatic life as well as in human bodies. Excess intake of fluoride by human being may leads to dental caries, bone fluorosis, and lesions of the thyroid, endocrine glands, and brain [5]. Fluorosis can attack the major organ of the human body like neck, spine, pelvic and shoulder joints and small joints of hands and feet etc. Because of these reasons the pollution of ground water by fluoride contamination has been a major concern. Various treatment techniques have been developed commercially such as, Membrane filtration [6], precipitation [7], nanofiltration [8], ion-exchange [9], electrocoagulation flotation [10], and adsorption [11] have been used for fluoride removal but adsorption is worth mentioning amongst all. The possible reason lye in the fact that adsorption can be applied for the removal of fluoride even at low concentrations. In the recent years an extensive research has been made on the removal of fluoride by using natural, synthetic, and biomass materials such as activated alumina [12], fly ash [13], alum sludge [14], chitosan beads [15,16], red mud [17], zeolite [18], calcite [19], hydrated cement [20], attapulgite [21], and acid-treated spent bleaching earth [22].

But widespread uses of some of these adsorbents limits due to their high cost and difficulty of preparation. Therefore use of a low cost adsorbent such as wood based activated carbon could be a better alternative. In the present study batch adsorption of fluoride was done from its aqueous solution by using Acacia Auriculiformis wood based activated carbon. The activated carbon was prepared by microwave activation of the char prepared by carbonization of Acacia Auriculiformis scrap wood. A batch adsorption study was carried out at various experimental conditions, including different pH, initial fluoride concentrations, adsorbent concentrations, different competitor anions, and different temperatures. In order to investigate the mechanism of fluoride removal various adsorption isotherms were also studied at different temperatures.

MATERIALS AND METHODS

2.1. Raw materials
The scrap wood of Acacia Auriculiformis selected for this work, was collected from local saw mill. Methylene blue (MB), hydrochloric acid and ammonia were procured from Merck Specialities Private Limited, Mumbai, India.

2.2. Preparation of char
The char was prepared by carbonization of Acacia Auriculiformis scrap wood in an inert atmosphere. The wood scrap was first cut into small pieces of 2 mm width and 40 mm of length, cleaned with distilled water and was sun dried for 24 h prior to the carbonization. The wood pieces were kept on a ceramic boat which was placed at the center of a 40-mm i.d tubular furnace. The material was then heated from ambient temperature to the carbonization temperature of 750 °C at the rate of 4 °C/min in a continuous flow of N_2 (300 ml/min) and then it was kept at this temperature for 1h for subsequent activation.

It was then allowed to cool to ambient temperature in presence of N_2 flow. The char (C750N) was sieved to obtain the desired size fractions and stored in a desiccator over silica gel.

_____

2.3.   Microwave-activation of char

The C750N was further activated in a domestic microoven (IF20PG3S) for five minutes at a constant input power of 800 W and a frequency of 2450 MHz. After treating in the microoven C750N was termed as AC750NMW5.

2.4. Characterization of activated carbon

The surface area and the total pore volume of the prepared char and the activated carbon were determined by using N_2 adsorption-desorption method by using Brunauer Emmett Teller (BET) apparatus (Autosorb-1, Quantacrome). The surface properties and the microporous structure were investigated by using Scanning Electron Microscope (SEM) (Hitachi, model SU-70).

2.5.   Adsorption equilibrium

The monolayer adsorption capacity of AC750NMW5 for fluoride was determined by the equilibrium study. The equilibrium study was carried out by adding 0.1 g of adsorbent into a series of 250 ml conical flask containing 100 ml solution of fluoride and was shaken in a mechanical shaker for 8 h at room temperature. After this the samples were centrifuged and the concentrations were analyzed in a fluoride electrode (Orion, 9606BNWP). The equilibrium adsorption capacity was calculated from the relationship

$$q_e = \frac{(C_0 - C_e)}{w}V$$

                                                                                                            (1)

where, q_e (mg/g) is the equilibrium adsorption capacity, C_e is the fluoride concentration at equilibrium (mg/*l*), *V* is the volume of solution (*l*) and *w* is the weight of adsorbent (g).

2.6.   Data analysis

The experimental data were analyzed using Origin Pro.(version 8) computer software. The goodness of fit was measured through the regression coefficient (R^2).

RESULTS AND DISCUSSION

3.1. Characterization of the prepared adsorbents

The BET surface area (S_{BET}), total pore volume (V_{tot}) and average pore size of C750N and AC750NMW5 were determined from the physical adsorption data of N_2 at 77 K and the values are shown in Table 1. It can be seen from Table 1 that AC750NMW5 has the highest surface area and total pore volume. Inside the microoven a high temperature could be reached in comparatively shorter period of time resulting dissipation of huge amount of energy at a molecular level. Consequently, the roughness of the pore walls may also be increased due to rapid heating with the formation of additional active sites [23]. Besides, rapid heating could accelerate the release of tar or volatile matter from the pore interior which results into higher pore volume [24]. The surface morphology of activated carbons was investigated through Scanning electron microscope (SEM) analysis. The SEM images of C750N and AC750NMW5 are shown in Figure 1a and 1b. It can be observed from Figure 1a that a typical honeycomb structure with pores of different size was formed on the surface of char (C750N) when it was treated at optimum condition. The similar surface morphology could also be observed when activated carbon was prepared from corncob by chemical activation [25]. The roughness of the interior pores of activated carbon was increased when it was further treated in a domestic microoven (Figure 1b).

Table-1 Comparison of surface properties of C750N and AC750NMW5

Adsorbent	Surface area (m^2/g)	Total pore volume (cc/g)	Average pore diameter (Å)
C750N	514.2	0.36	27.99
AC750NMW5	695	0.50	28.55
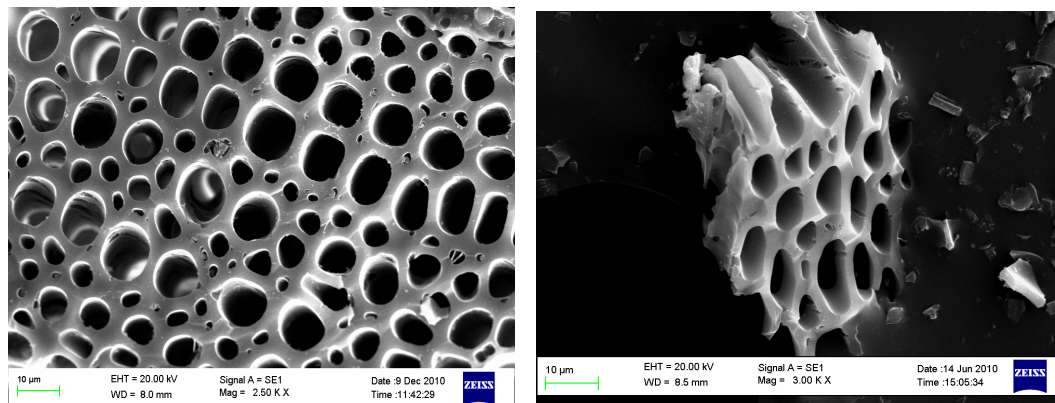
Fig 1. The SEM image of (a) C750N (b) AC750NMW5

3.2. Equilibrium study

In order to establish an appropriate relationship between the adsorption capacity (q$_e$) and fluoride concentration (C$_e$) at equilibrium by using AC750NMW5, the data were fitted to Freundlich, Langmuir, Tempkin and Harkins-Jura isotherms. The Langmuir isotherm represents the unimolecular adsorption of the adsorbate molecule on the adsorbent surface [26]. The model can be expressed as:

$$\frac{1}{q_e} = \frac{1}{K_l Q_m} + \frac{1}{Q_m} \tag{2}$$

where, K_l is the Langmuir constant related to the energy of adsorption (l /mg) and Q_m is the maximum amount of adsorption corresponding to complete the monolayer coverage on surface (mg/g). Similarly, the Freundlich isotherm can be used for non-ideal sorption that involves heterogeneous surface energy systems [27, 28] and is expressed by the following equation:

$$q_e = K_F (C_e)^{1/n} \tag{3}$$

where, K_F is a rough indicator of the adsorption capacity and $1/n$ is the adsorption intensity. In general, with the increase of the adsorption capacity K_F value increases. The Tempkin isotherm describes the heat of adsorption and interaction between adsorbent-adsorbate molecules [29]. The Tempkin isotherm can be expressed as:

$$q_e = B_1 \ln k_T + B_1 \ln C_e \tag{4}$$

where, k_T and B_1 are Tempkin isotherm constant.

The Harkins–Jura adsorption isotherm can be expressed by the following equation [30]:

$$\frac{1}{q_e} = \left(\frac{B_2}{A}\right) - \left(\frac{1}{A}\right)\log C_e \qquad (5)$$

where, B_2 and A are the isotherm constants.

The Harkins–Jura adsorption isotherm tells about the multilayer adsorption which is explained with the existence of a heterogeneous pore distribution. The experimental data fitted to different isotherms at three different temperatures are shown in Fig.2a-c. It can be seen that Langmuir isotherm fitted well in each case. Besides, the values of the different equilibrium constants are shown in Table 2.

Table-2 Equilibrium model constant at different temperatures

Isotherm	Isotherm-equations	Temperature (K)		
		303	313	32
Langmuir	$q_e = \dfrac{C_e K_l Q_0}{1 + K_l C_e}$			
K_l (1/mg)		0.869	0.9611	1.0102
Q_0 (mg/g)		18.95	19.24	19.26
R^2		0.9966	0.9941	0.9941
Freundlich	$q_e = K_F(C_e)^{1/n}$			
1/n		0.3126	0.2987	0.2982
K_F (1/mg)		9.5484	10.110	10.269
R^2		0.9953	0.9882	0.9891
Tempkin	$q_e = B_1 \ln k_T + B_1 \ln C_e$			
B_1		4.036	4.030	4.020
k_T		9.628	11.194	11.876
R^2		0.9964	0.9913	0.9918
H-J	$\dfrac{1}{q_e} = \left(\dfrac{B_2}{A}\right) - \left(\dfrac{1}{A}\right)\log C_e$			
A		271.266	309.247	306.68
B_2		2.653	2.7306	2.6712
R^2		0.9919	0.9810	0.9829

3.3. Nonlinear analysis and error estimation of different isotherms
The isotherm was analyzed nonlinearly and the corresponding values of isotherm parameters are summarized in Table 3. The adjusted–R squared was a goodness-of-fit measure in multiple regression analysis that penalized additional explanatory variables by using a degrees of freedom adjustment in estimating the error variance. It is noted that the Langmuir adsorption isotherm is the best correlated one with a high R^2 value (0.9966). The chi-square value (χ^2) is a test statistic that is calculated as the sum of the squares of observed values minus expected values divided by the expected values. The χ^2 can be expressed in the following way:

$$\chi^2 = \frac{(Q_e - Q_{em})^2}{Q_{em}} \qquad (6)$$

540

The chi-square values of different isotherms are given in Table 3. In statistics, the sum of squares (SSE) is a quantity used in describing how well a model, often a regression model, represents the data being modelled. In particular, it measures the variation in the modelled values. The total sum of squares, measures the variation between the observed data and to the residual sum of squares. The residual sum of squares (RSE) measures the variation in the modelling errors. Therefore the sum of squares error is the sum of the squares of the deviations of the predicted values from the mean value of a response variable, in a standard regression model. A test statistic that is calculated as the sum of the squares of observed values minus expected values divided by the expected values.
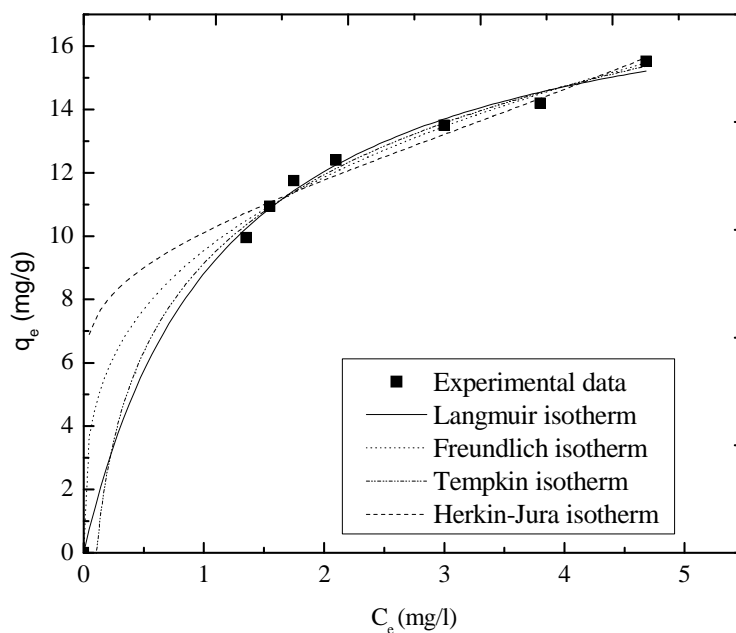
(a)
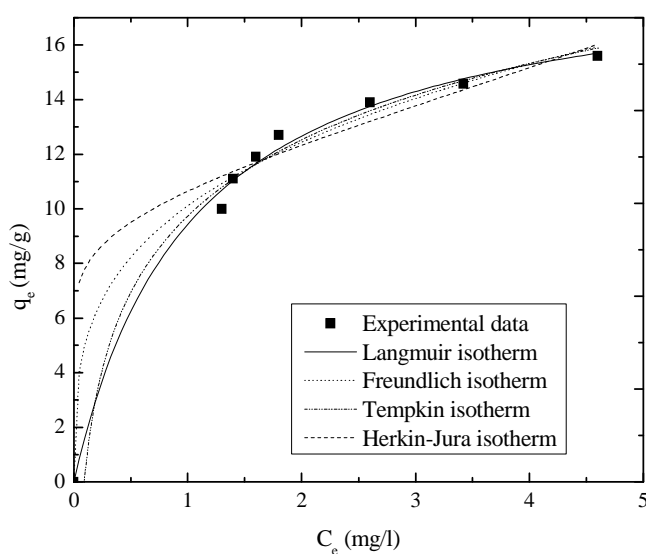
(b)

_____
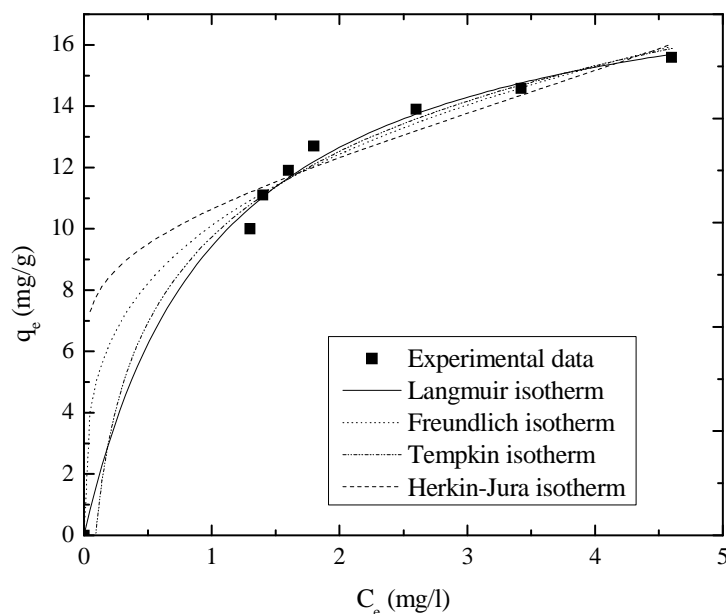
(c)
Fig. 2. Equilibrium isotherms at different temperatures (a) 30 °C (b) 40 °C (c) 50 °C

Table 3 Nonlinear analysis of different isotherm

Isotherm	Statistical parameters	30 °C	40 °C	50 °C
Langmuir	R^2	0.9966	0.9941	0.9941
	χ^2	0.0772	0.1424	0.1438
	Q_0-error	0.5484	0.7228	0.7096
	K_l-error	0.0780	0.1126	0.1173
	RSE	0.4926	0.8544	0.8625
Freundlich	R^2	0.9953	0.9882	0.9891
	χ^2	0.1083	0.2827	0.2654
	K_F-error	0.2269	0.3406	0.3220
	n-error	0.0221	0.0335	0.0320
	RSE	0.64975	0.2827	
Tempkin	R^2	0.9964	0.9913	0.9918
	χ^2	0.0821	0.2081	0.1989
	B_1-error	0.2471	0.3875	0.3722
	k_T-error	1.8641	3.4574	3.5716
	RSE	0.4926	1.25	1.1935
Herkin-Jura	R^2	0.9919	0.9810	0.9830
	χ^2	0.1871	0.4548	0.4131
	A-error	26.766	46.702	43.816
	B-error	0.1489	0.2523	0.2333
	RSE	1.1225	2.729	2.4787

3.4. Effects of various adsorption parameters
3.4.1. Effect of pH
The adsorption of fluoride was studied over a pH range of 2.5 to 7 as shown in Fig. 3. The effect of pH on fluoride adsorption was studied at an initial fluoride concentration (C_0) of 10 mg/l with an adsorbent dose (m) of 1 g/l. It was seen from Fig. 3 that the fluoride removal increased with decrease in pH values and as the pH was increased from 2.5 to 7, the fluoride removal efficiency was decreased from 81.7% to 57%. The adsorption of other ions gets affected due to the strong

affinity for H^+ and OH^- ions on the adsorption sites. Because of higher H^+ ion concentrations at lower pH the negative charges on the adsorbent surface get neutralized. This is in turn reduces the hindrance to diffusion of negatively charged fluoride ions and gives rise to the more active surface for adsorption [31]. However, no appreciable increase in fluoride removal was observed within a pH range of 2.5 to 4.4. It may be ascribed to the fact that initially at lower pH, the formation of weak hydrofluoric acid took place which retards the rate of fluoride adsorption. The maximum fluoride removal was achieved at a pH of 4.4. Therefore an initial pH of 4.4 was selected for the rest of the adsorption study.
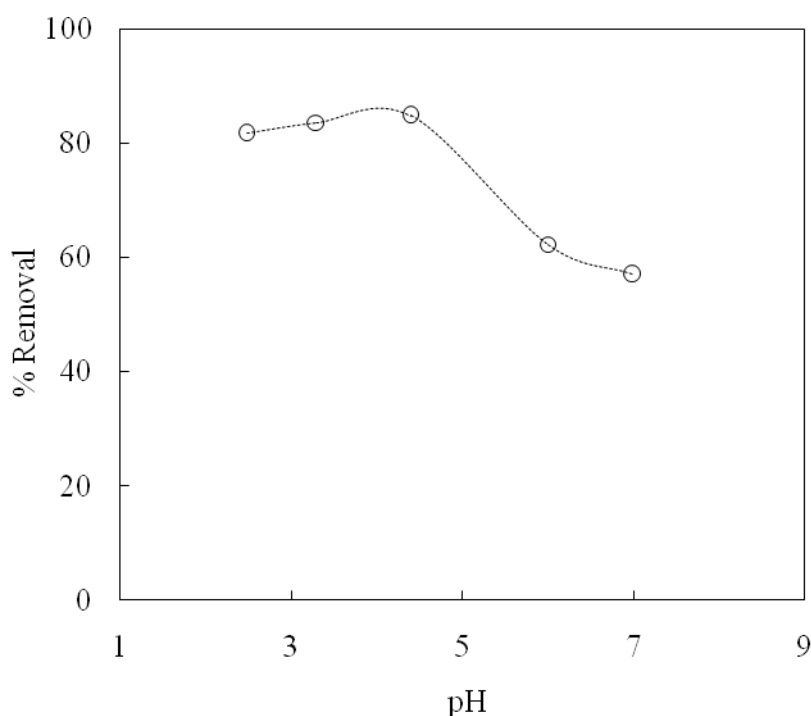
Fig. 3. Effect of pH for the adsorption of fluoride onto activated carbon (C_0=10 mg/l, m=1 g/l, temperature= 30 °C)

3.4.2.   *Effect of contact time and initial concentrations*
The effect of agitation time and initial concentration on the adsorption of fluoride ions is shown in Fig. 4. It was quite evident from Fig. 4 that the uptake of fluoride ions increased with the lapse of time and reached to saturation after 20 minute. It was further revealed that, the percentage fluoride removal was decreased with the increase in initial concentration of fluoride. At higher fluoride concentration the availability of active sites on the adsorbent is less which causes lower adsorption efficiency [32]. So it can be concluded that the percentage uptake is highly dependent on initial concentration of fluoride ions. The plot of the fluoride ions uptake versus time curves is single, smooth and continuous leading to saturation which indicates the possible monolayer coverage of fluoride ions on the surface of the adsorbent [33].

3.4.3.   *Effect of adsorbent dose*
The percentage uptake of fluoride as a function of adsorbent dose at an initial F^- ion concentration and at temperature of 10 mg/l and 30 °C is shown in Fig. 5. The pH of the solution was kept constant at 4.4. The adsorbent dosages was varied from 1 g/l to 2 g/l and equilibrated for 120 min. The percent removal of fluoride increased with increase in adsorbent dose and a maximum removal of 97.2% was obtained with an adsorbent dose of 2 g/l. The higher removal capacity at higher adsorbent dose attributed to the availability of more effective surface area of the prepared adsorbent for adsorption [34].

_____
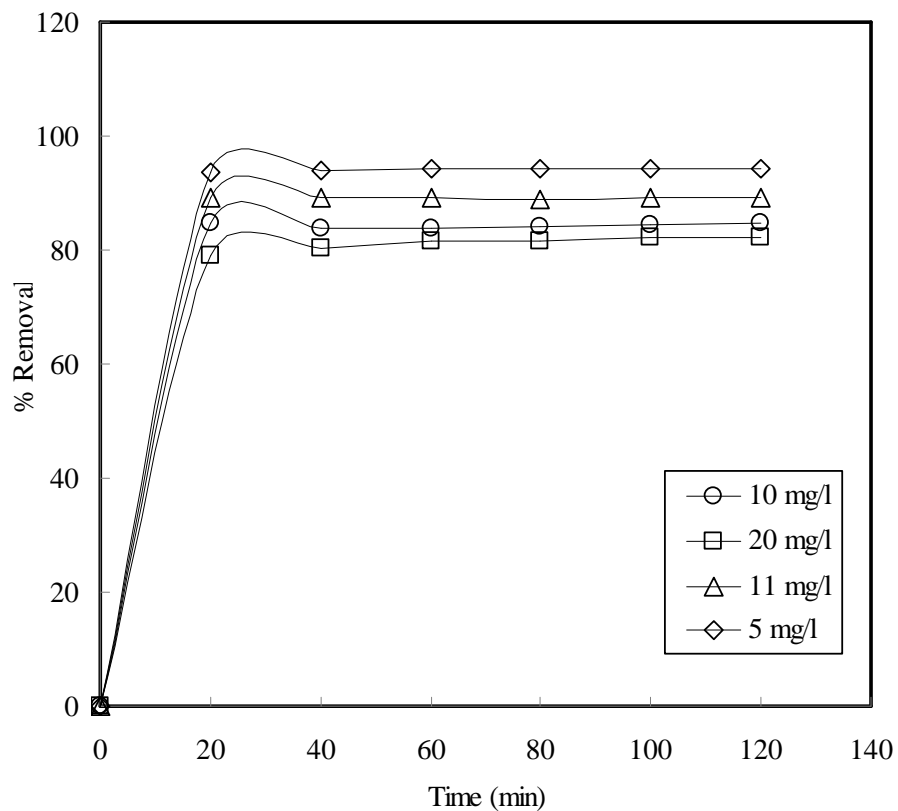
Fig. 4. Effect of agitation time and initial concentration (mg L−1) for the adsorption of fluoride onto activated carbon (pH = 4.4, m =1 g/l, temperature = 30 °C)
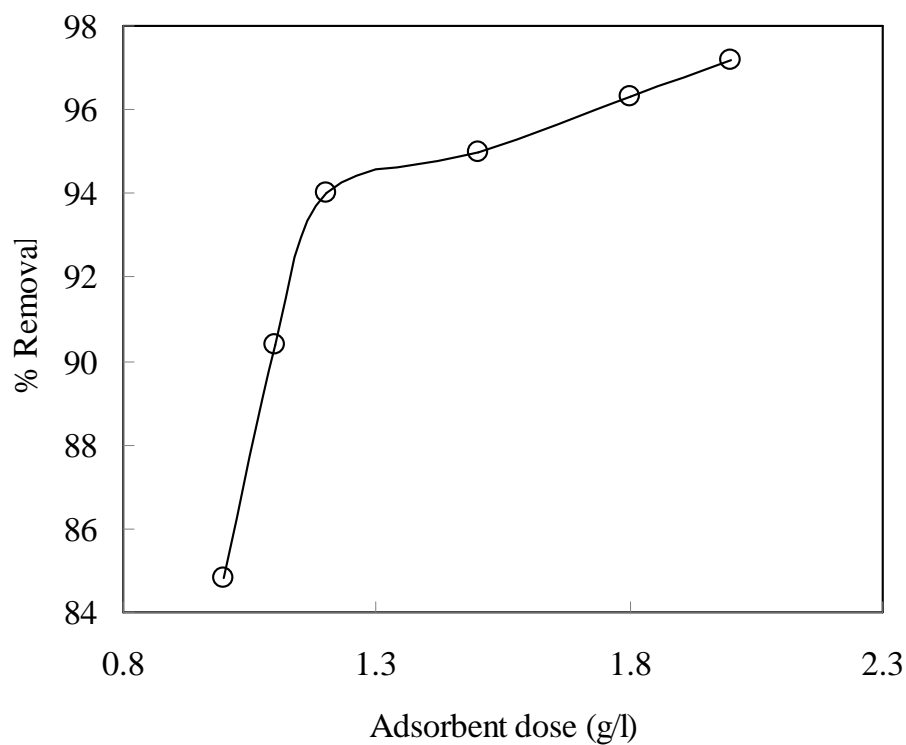
Fig. 5. Effect of adsorbent dose (g/l) for the adsorption of fluoride onto activated carbon (C$_0$=10 mg/l, m=1 g/l, pH = 4.4, temperature= 30 °C)

3.4.4. Effect of particle size

The de fluoridation of F̄ion were carried out at four different particle size namely 58–149, 149-177, 177-250 and 250–595 μm as shown in Fig. 6. It was interesting to note that the adsorption of fluoride increased with decreasing particle size. A maximum removal efficiency of 84.8% was achieved with a particle size of 58 μm. With decrease in particle size the availability of more specific surface area increases, which leads to increasing adsorption efficiency [35]. Hence, the particle size of 58μm was chosen for further experiments.
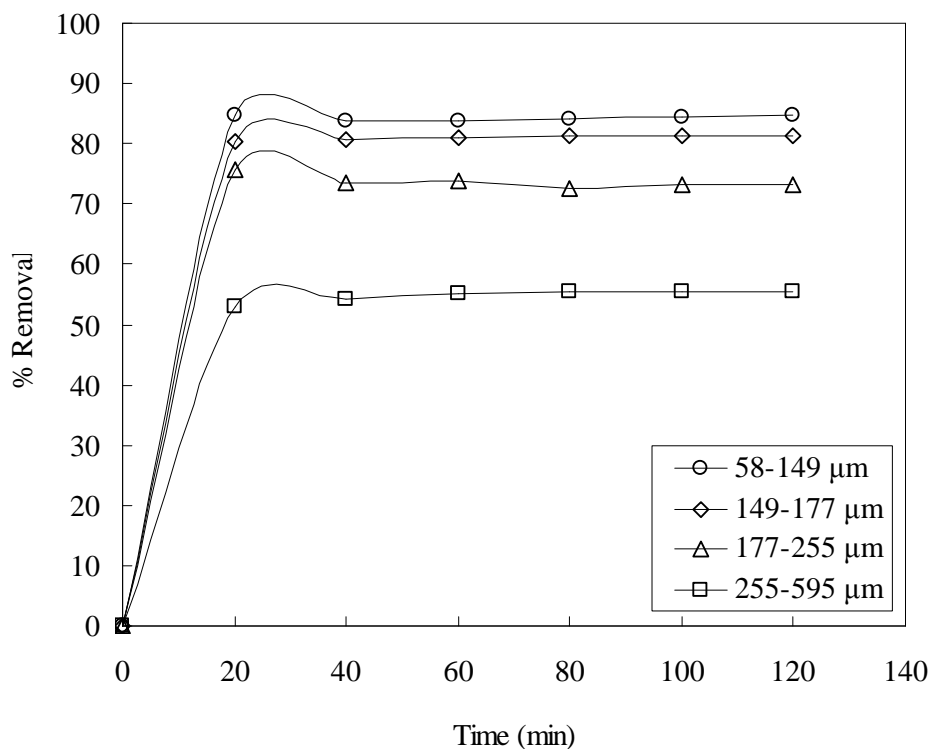
Fig. 6. Effect of particle size (μm) for the adsorption of fluoride onto activated carbon (C_0 =10 mg/l, m=1 g/l, pH = 4.4, temperature= 30 °C)

3.4.5. Effect of Interfering co-ion

The effect of coexisting anion such as chloride on fluoride adsorption was studied by varying the chloride ion concentration from 0.01 M-1.0 M. The initial concentration and temperature was fixed at 10 g/l and 30 °C respectively. The adsorbent dose was 1 g/l while the pH was kept constant at 4.4. The effect of chloride on the percent removal of fluoride is shown in Fig. 7. It can be depicted from Fig. 7 that the removal of fluoride decreased with increase in NaCl concentration from 0.01 to 1M. The added NaCl acted as an inhibitor or a radical scavenger, which retards the rate of fluoride adsorption. As sodium chloride dissociates into sodium and chloride ions in water; each ion is hydrated with many water molecules and the water molecules available for dissolution of the fluoride ion decreases with the decrease of fluoride ion concentration in the adsorbate solution.

Simultaneously, the adsorbent surface becomes more basic due to presence of Na^+ and H^+ ions which in turn decelerate the rate of fluoride adsorption [36].

_____
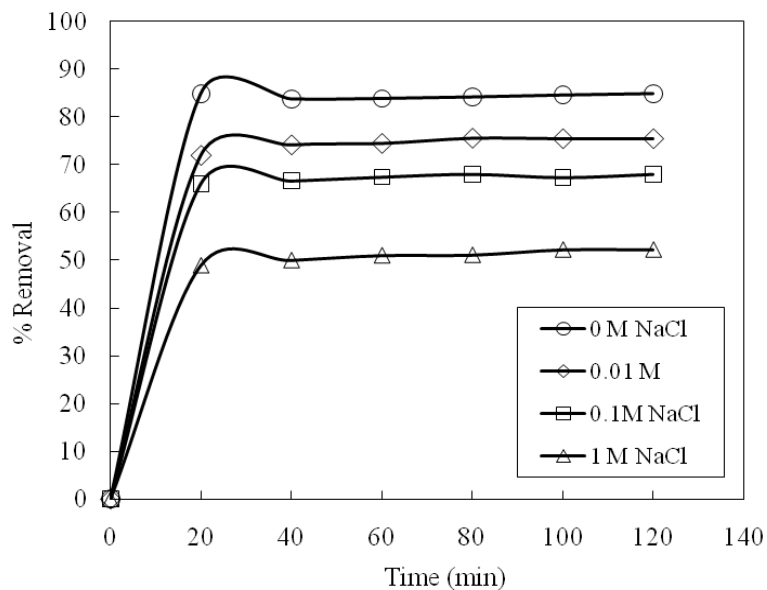
Fig. 7. Effect of chloride ion concentration (M) for the adsorption of fluoride onto activated carbon ($C_0 =10$ mg/l, m=1 g/l, pH = 4.4, temperature= 30 °C)
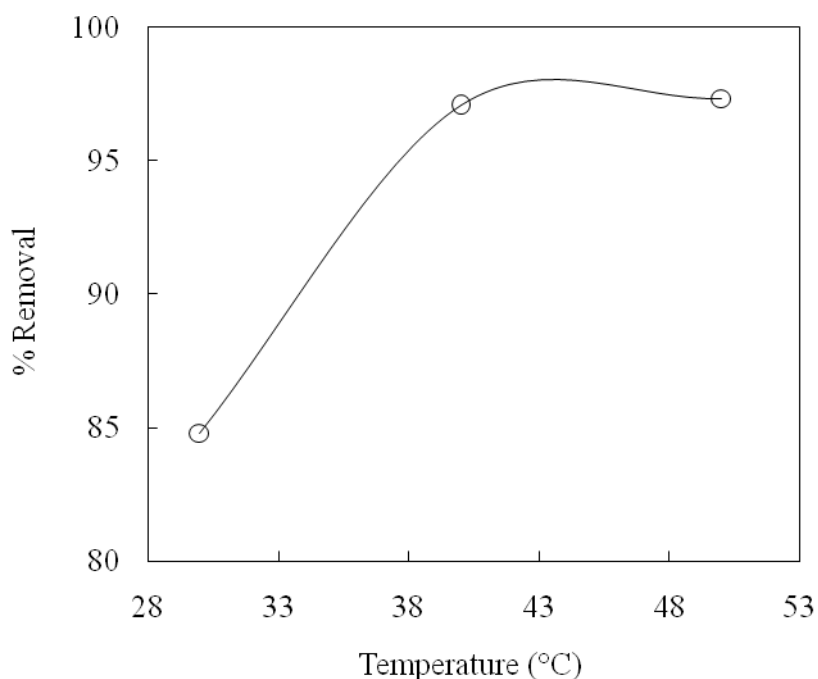
Fig. 8. Effect of particle size (µm) for the adsorption of fluoride onto activated carbon ($C_0 =10$ mg/l, m=1 g/l, pH = 4.4, temperature= 30 °C)

3.4.6. Effect of temperature
The percentage uptake of fluoride is highly dependent on temperature.The effect of temperature on percent adsorption of fluoride was studied at three different temperatures such as, 30 °C, 40 °C and 50 °C. It was seen from Fig. 8 that the percentage adsorption of fluoride increased from 84.8 to 97.33 % when the temperature was increased from 30 °C to 40 °C. This may be attributed to the fact that at higher temperature the rate of adsorption gets accelerated which in turn indicated the endothermic nature of reaction [37].

_____

3.5. Thermodynamic study

The change in standard Gibb's free energy (ΔG), enthalpy (ΔH) and entropy (ΔS) were evaluated from the thermodynamic study. The nature of adsorption process was further analyzed through thermodynamic study [38]. The changes in Gibb's free energy, enthalpy and entropy at standard state were determined. The Gibb's free energy (ΔG) can be obtained from the following equation:

$$\Delta G = -RT \ln K_l \tag{7}$$

Where, R is the universal gas constant (8.314 J/mol- K), K_l is the adsorption equilibrium constant (Eq. 6) and T is the absolute temperature (K). Besides, other parameters such as enthalpy change (ΔH), and entropy change (ΔS), were determined from Van't Hoff equation:

$$\ln K_l = \frac{\Delta S}{R} - \frac{\Delta H}{RT} \tag{8}$$

The values of these thermodynamic parameters are presented in Table 4. The negative values of ΔG (kJ/mol) indicate the spontaneity of the adsorption reaction. On the other hand, the endothermic nature of the adsorption process is characterized by the positive values of ΔH (kJ/mol). The randomness at the solid/liquid interface during sorption of fluoride by activated carbon of the adsorption reaction is reconfirmed by the positive value of ΔS (J/mol-K). It may be because of the adsorbed water molecules gain more translational entropy than that is lost by the adsorbate fluoride molecules which increase the randomness of the process [39]. This phenomenon also indicates the increase of disorderness of the system with changes in the hydration of adsorbing fluoride ions [40].

Table 4 The values of thermodynamic parameters.

| Temperature | Thermodynamic parameters | | | |
	ΔH (k.	ΔS (J/mol-K)	ΔG (kJ/mol)	R^2
303		19.02	-0.351	0.970
313	6.094		-0.103	
323			0.027	

3.6. Kinetic study

3.6.1. Pseudo first and second order rate kinetics

Pseudo-first-order and pseudo-second-order mechanism was investigated in order to propose adsorption kinetic model [41, 42]. They can be expressed by Eq. (9) and (10)

$$\log(q_e - q_t) = \log q_e - \frac{k_1 t}{2.303} \tag{9}$$

$$\frac{t}{q_t} = \frac{1}{k_2 q_e^2} + \frac{t}{q_e} \tag{10}$$

Where, q_t and q_e are the amount of adsorbed fluoride (mg/g) at time t and at equilibrium time, respectively. k_1 and k_2 are rate constants for first-order and second-order reaction. The kinetic data evaluated at various experimental conditions are shown in Table 5. In case of pseudo Second order rate kinetics the value of correlation coefficient ($R^2 = 0.9999$) is much accurate in compare to the first order rate kinetics. Therefore, it may be concluded that the adsorption of fluoride followed a second-order kinetic model.

Table 5 Values of kinetic parameters at different experimental conditions

C0 (mg/l)	T (°C)	PS (μm)	m (g/l)	Pseudo 1st order			Pseudo 2nd order		
				k_1 (1/min)	q_e (mg/g)	R^2	k_2 (g/mg-min)	q_e (mg/g)	R^2
10	30	58	1	0.0009	1.66	0.967	0.2715	8.489	0.9999
5	30	58	1	0.0589	3.66	0.8483	1.24	4.72	1.0000
10	40	58	1	0.0707	7.57	0.9025	3.65	9.71	1.00
10	50	58	1	0.0631	7.77	0.8929	1.16	9.74	1.00
20	30	163	1	0.0193	14.69	0.9423	0.116	11.93	0.9999
20	30	422.5	1	0.0311	13.85	0.9097	0.0369	11.33	0.9994
20	30	58	1.2	0.0265	13.80	0.9036	0.1057	12.17	0.9999
20	30	58	2.0	0.0010	11.67	0.9554	0.016	5.56	0.9971

3.6.2 Intraparticle diffusion
An intraparticle diffusion model was also studied to identify the rate defining step for adsorption [43]. The intraparticle model can be evaluated from the rate kinetic data taken at various experimental conditions. The intraparticle model can be expressed as

$$q_t = k_i t^{0.5} \qquad\qquad (11)$$

where q_t is the amount adsorbed (mg/g) at a given time t (min) and k_i (mg/g min$^{0.5}$) is the intraparticle diffusion rate constant.
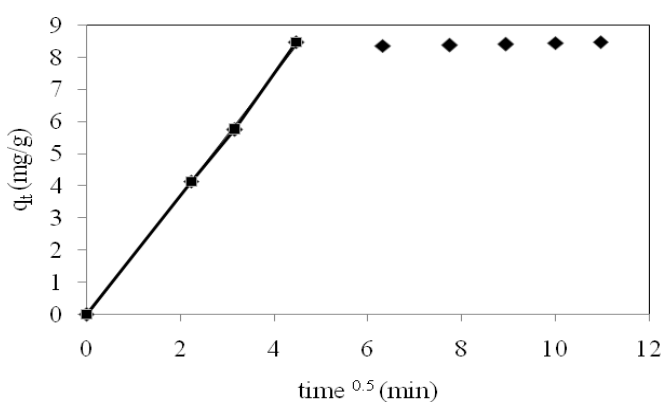
Fig. 9. Itraparticle diffusion model

The plot of the quantity of the fluoride adsorbed against the square root of time is shown in Fig. 9. If the plot is linear and pass through the origin then intraparticle diffusion is a rate-controlling step otherwise the plot will reflect a three phase nature., namely an initial linear portion followed by an intermediate linear portion and a plateau. The first linear portion implied the external surface adsorption (stage 1) during the first 20 min. Then a stage of intraparticle diffusion (stage 2) was attained and continued up to 80 min. Finally, an equilibrium adsorption (stage 3) was reached. The transportation of fluoride was caused through diffusion into the particles and finally retained in the internal pores. The rate constant of intraparticle diffusion was calculated to be 1.822 mg/g min0.5 for fluoride.

___

3.7 Comparison of adsorption capacity of different adsorbents

The maximum adsorption capacity of AC750NMW5 was compared with the adsorption capacities of different adsorbents of previous literature and it was found that AC750NMW5 had better adsorption capacity for fluoride in comparison to the other adsorbents [Table 6].

Table 6 Comparison of monolayer adsorption capacity of AC750NMW5 with other adsorbents for fluoride

Adsorbate	Adsorbent	Adsorption Capacity (mg/g)	References
Fluoride	Rice Husk	0.019	Wahecd et.al., 2009
Fluoride	Groundnut Shell	2.32	Veeraputhiran, et al., 2011
Fluoride	Cynodon Dactylon	4.617	Alugumuthu et al, 2010
Fluoride	Present adsorbent	18.95	Present work

CONCLUSION

It can be concluded that the adsorbent AC750NMW5 prepared from Acacia Auriculiformis scrap wood has shown better adsorption capacity for fluoride in comparison to other adsorbents. The adsorptive removal of fluoride increased with decrease pH value and the maximum fluoride removal occurred at a pH of 4.4. Besides, the fluoride removal increased with increasing contact time, temperature and adsorbent doses but with decrease in particle size. The presence of chloride ion reduced the rate of F ⁻ ion diffusion to the surface of the prepared adsorbent. It was further observed that the equilibrium behaviour can be well predicted by Langmuir adsorption isotherm.

REFERENCES

[1] A.K. Susheela, *Current Science*, **1999**, 77, 1250–1256.

[2] M. Bishnoi, S. Arora, *India, J. Environ. Biol.,* **2007**, 28, 291-294.

[3] K. Shailaja, M. E. C. Johnson, *J. Environ. Biol.,* **2007**, 28, 2, 331-332.

[4] A. Toyoda, A. Taira, IEEE Trans, *Semiconductor. Manufacture*, **2000**, 13, 3, 305–309.

[5] S.S. Tripathy, J-L. Bersillon, K. Gopal, *Sep. Purif. Technol*., **2006**, 50, 3, 310–317.

[6]] P.I. Ndiaye, P. Moulin, L. Dominguez, J.C. Millet, F. Charbit, *Desalination*, **2005**, 173, 25-32.

[7] N. Pathasarathy, J. Buffle, W. Haerdi, *Can. J. Chem.,* **1986**, 64,1, 24–29.

[8] R. Simons, *Desalination*, **1993**, 89, 3, 325–341.

[9] L. Ruixia, G. Jinlong, T. Hongxiao, *J. Colloid Interface Sci.,* **2002**, 248, 268–274.

[10] C.Y. Hu, S.L. Lo, W.H. Kuan, Y.D. Lee, *Water Res.,* **2005**,39,895–901.

[11] D. Mohapatra, D. Mishra, S.P. Mishra, G.R. Chaudhury, R.P. Das, *J. Colloid Interface Sci.,* **2004**, 275, 2, 355–359.

[12] S. Ayoob, A.K. Gupta, P.B. Bhakat, V.T. Bhat, *Chem. Eng. J*., **2008**, 140, 6 –14.

[13] A.K. Chaturvedi, K.P. Yadava, K.C. Pathak, V.N. Singh, *Air Soil Pollut*., **1990**, 49, 1-2, 51–61.

[14] M.G. Sujana, R.S. Thakur, S.B. Rao, *J. Colloid Interface Sci.,* **1998**, 275, 355–359.

[15] N. Viswanathan, C.S. Sundaram, S. Meenakshi, *J. Hazard. Mater*., **2009**, 161, 423–430.

[16] N. Viswanathan, S. Meenakshi, *J. Colloid Interface Sci.* ,**2008**, 322, 375–383.

[17] A. Tor, N. Danaoglu, G. Arslan, Y. Cengeloglu, *J. Hazard. Mater*.,**2009**, 164, 271–278.

[18] M.S. Onyango, Y. Kojima, O. Aoyi, E.C. Bernardo, H. Matsuda, *J. Colloid Interface Science,* **2004**, 279, 2, 341–350.

[19] M. Yang, T. Hashimoto, N. Hoshi, H. Myoga, *Water. Res*., **1999**, 33, 16, 3395–3402.

[20] N.I. Chubar, V.F. Samanidou, V.S. Kouts, G.G. Gallios, V.A. Kanibolotsky, V.V. Strelko, I.Z. Zhuravlev, *J. Colloid Interf ace Sci.,* **2005**, 291, 67–74.

[21] J. Zhang, S. Xie, Y.S. Ho, *J. Hazard. Mater.*,**2009**, 165, 218–222.

[22] M. Mahramanlioglu, I. Kizilcikli, I.O. Bicer, *J. Fluorine* Chem., **2002**, 115, 1–47.

[23] L. Huang, Y. Sun, W. Wang, Q. Yue, T. Yang, *Chem. Eng. J.,* **2011**, 171, 3, 1446-1453.

[24] Q.S. Liu, T. Zheng, P. Wang, L. Guo, *Ind. Crops Prod.*, **2010**, 31, 2, 233–238.

[25] R.L. Tseng, *J. Coll. Interf. Sci.*,**2006**, 303, 2, 494–502.

[26] Q. Liu, H. Guo, Y. Shan, *J. Fluor. Chemistry*, **2010**, 131, 635–641.

[27] Y.S. Ho, A.E. Ofomaja, *Biochem. Eng. J.*, **2006**, 30,117–123.

[28] S. Hong, C. Wen, J. He, F. Gan, Y.S. Ho, *J. Hazard. Mater.*, **2009**, 167, 630–633.

[29] A. Ergene, K. Ada, S. Tan, H. Katircioglu, *Desalination*, **2009**, 249, 3, 1308–1314.

[30] C.A. Basar, *J. Hazard. Mater.*, **2006**, 135, 1-3, 232–241.

[31] G. Karthikeyan, S.S. Ilango, *J. Environ. Health. Sci. Eng.,* **2007**, 4, 1, 21-28.

[32] B. Stephen Inbaraj, N. Sulochana, *Indian J. Chem. Technol.*, **2002**, 9, 201.

[33] G.N. Manju, C. Raji, T.S. Anirudhan, *Water Res.*,**1998**, 32, 10, 3062.

[34] V. Aravind, K.P. Elango, *Ind. J. Chem. Tech.,* **2006**, 13, 476-483.

[35] G. Alagumuthu, V. Veeraputhiran, R. Venkataraman, *Archiv.Appl. Sci.Res.*, **2010**, 2, 4, 170-185.

[36] B.K. Nandi, A. Goswami, M.K. *Purkait, Appl. Clay Sci.*, **2009**, 42, 3-4, 583–590.

[37] G.A.M. Rajan, *Hem. Ind.*, 2010, 64, 4 , 295-304.

[38] N. Viswanathan, S. Meenakshi, *J. Hazard. Mater.*, **2010**, 178, 1-3, 226–232.

[39] S. Arivoli, M. Thenkuzhali, *E Journal of Chemistry*, **2008**, 5, 2, 187-200.

[40] E. Eren, *J. Hazard. Mater.*, **2008**, 159, 235–244.

[41] S. Lagergren, K. Svenska, K. S. Vetenskapsad, *Handl.*, **1898**, 24, 4, 1–39.

[42] Y.S. Ho, G. Mckay, Pseudo-second order model for sorption processes, Process Biochem. 34 (**1999**) 451–465.

[43] W.J. Weber Jr., J.C. Morris, *J. Sanit. Eng. Div. ASCE*, **1963**, 89, 31–59.

[44] Wahecd, S. Deshmukh, S.J. Attar, M.D. Waghmare, *Nature Environment and. Pollution Technology*, **2009**, 8, 2, 217-223.

[45] V. Veeraputhiran, G. Alagumuthu, *Res. J. Chem. Sci.*, **2011**, 1, 4, 49-54.

[46] G. Alagumuthu, V. Veeraputhiran, R. Venkataraman, *Arch.Appl. Sci. Res.*, **2010**, 2, 4, 170-185.